J. Fluid Mech. (1982), *vol.* 119, *pp.* 367–377
Printed in Great Britain

On parametric instabilities of finite-amplitude internal gravity waves

By J. KLOSTERMEYER
Max-Planck-Institut für Aeronomie, 3411 Katlenburg-Lindau, FRG

(Received 17 June 1981 and in revised form 5 October 1981)

The equations describing parametric instabilities of a finite-amplitude internal gravity wave in an inviscid Boussinesq fluid are studied numerically. By improving the numerical approach, discarding the concept of spurious roots and considering the whole range of directions of the Floquet vector, Mied's work is generalized to its full complexity. In the limit of large disturbance wavenumbers, the unstable disturbances propagate in the directions of the two infinite curve segments of the related resonant-interaction diagram. They can therefore be classified into two families which are characterized by special propagation directions. At high wavenumbers the maximum growth rates converge to limits which do not depend on the direction of the Floquet vector. The limits are different for both families; the disturbance waves propagating at the smaller angle to the basic gravity wave grow at the larger rate.

1. Introduction

The occurrence of parametric instabilities in finite-amplitude internal gravity waves has been studied in great detail by McEwan & Robinson (1975), Mied (1976) and Drazin (1977). The process involves the forcing of disturbance waves at the frequency of a basic wave so that its time dependence is described by differential equations with periodic coefficients. McEwan & Robinson confined themselves to disturbance waves with length scales much smaller than the basic wavelength, so that the differential equations can be reduced to Mathieu's equation, whose properties are well-known (e.g. Abramowitz & Stegun 1965). Mied extended the analysis of McEwan & Robinson without making any restriction on the disturbance length scales and obtained two coupled partial differential equations with periodic coefficients. They can be solved numerically by the method of truncated Fourier series, which has also been successfully applied to stability studies of planetary waves and gravity-wave-associated resonance effects in the ionosphere (Lorenz 1972; Gill 1974; Mied 1978; Klostermeyer 1978).

The present work is an extension of Mied's (1976) investigations. Therefore the theoretical approach outlined in §2 will parallel his ideas. In §3, we briefly describe an efficient method for solving the governing equations and re-examine some of his results. The method of solution allows us, in particular, to study the behaviour of maximum growth rates for Fourier components up to $n = 10$ at several directions of the Floquet vector (§4).

2. Theoretical approach

Mied (1976) starts with the two-dimensional nonlinear equations describing the stream function and buoyancy in an inviscid Boussinesq fluid with constant Brunt–Väisälä frequency. The finite-amplitude internal gravity wave is assumed to be plane and harmonic, and thus represents an exact solution of the nonlinear equations. The total stream function and buoyancy fields are expressed as the sum of the basic wave and a perturbation. Substituting the total fields into the governing equations and neglecting nonlinear terms, one obtains two coupled linear differential equations with periodic coefficients for the perturbations of the stream function and buoyancy.

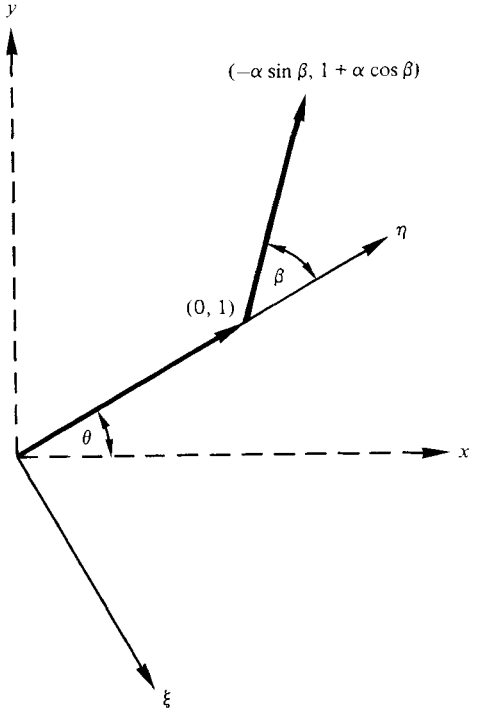

FIGURE 1. Propagation vector of basic gravity wave (0, 1), and Floquet vector $(-\alpha \sin\beta, \alpha\cos\beta)$, in (ξ, η)-co-ordinates (after Mied 1976).

The equations can be simplified by introducing non-dimensional variables x, y, t, ψ and b:

$$(\tilde{x}, \tilde{y}) = k^{-1}(x, y), \quad \tilde{t} = N^{-1}t, \quad \tilde{\psi} = k^{-2}N\psi, \quad \tilde{b} = k^{-1}N^2 b,$$

where $\tilde{x}$ and $\tilde{y}$ are the horizontal and vertical co-ordinates, $\tilde{t}$ is time, and $\tilde{\psi}$ and $\tilde{b}$ are the perturbations of the stream function and buoyancy. In addition, k and N denote respectively the wavenumber of the basic gravity wave and the Brunt–Väisälä frequency. Further simplication is obtained by using a rotated rectangular co-ordinate system (ξ, η) whose η-axis points in the direction of the basic-state wavenumber vector

$$\xi = x\sin\theta - y\cos\theta, \quad \eta = x\cos\theta + y\sin\theta,$$

where θ is the angle between the horizontal and the propagation vector (figure 1).

The equations admit a separable Floquet solution of the form

$$(\psi, b) = \exp\left[i(-\alpha \sin\beta\xi + \alpha\cos\beta\eta) + \lambda t\right] \sum_{n=-\infty}^{\infty} (\psi_n, b_n) \exp in\Phi, \tag{1}$$

where $\Phi = \eta - t\cos\theta$ is the phase angle of the basic gravity wave. We assume a solution that is bounded in space so that $|\alpha|$ can be interpreted as the magnitude of the Floquet vector propagating at an angle β to the basic-state wavenumber vector (figure 1). Then λ and (ψ_n, b_n) are in general complex and can be computed from the linear eigenvalue problem

$$\left.\begin{aligned} &p_{-1}\psi_{n-1} + (p_0 - \lambda)\psi_n + q_0 b_n + p_1\psi_{n+1} = 0, \\ &r_{-1}\psi_{n-1} + s_{-1}b_{n-1} + r_0\psi_n + (s_0 - \lambda)b_n + r_1\psi_{n+1} + s_1 b_{n+1} = 0. \end{aligned}\right\} \tag{2}$$

The coefficients $p_\nu, q_\nu, \ldots$ depend on n, α, β, θ and $M = Ak^2/2N$, where A is the amplitude of the basic-state stream function:

$$\begin{aligned} p_{-1} &= -\alpha M \sin\beta \frac{(\alpha\sin\beta)^2 + (\alpha\cos\beta + n - 1)^2 - 1}{(\alpha\sin\beta)^2 + (\alpha\cos\beta + n)^2}, \\ p_0 &= in\cos\theta, \\ p_1 &= \alpha M \sin\beta \frac{(\alpha\sin\beta)^2 + (\alpha\cos\beta + n + 1)^2 - 1}{(\alpha\sin\beta)^2 + (\alpha\cos\beta + n)^2}, \\ q_0 &= \frac{-i\alpha\sin\beta\sin\theta + i(\alpha\cos\beta + n)\cos\theta}{(\alpha\sin\beta)^2 + (\alpha\cos\beta + n)^2}, \\ r_{-1} &= -\alpha M\sin\beta, \quad r_0 = -i\alpha\sin\beta\sin\theta + i(\alpha\cos\beta + n)\cos\theta, \\ r_1 &= -r_{-1}, \quad s_{-1} = r_{-1}, \quad s_0 = p_0, \quad s_1 = -r_{-1}. \end{aligned}$$

To find growing disturbances with $\mathscr{R}(\lambda) = \lambda_r > 0$, (2) is considered for basic waves with vanishingly small amplitudes. It appears that the disturbance waves which can grow are those forming resonant triads with the basic wave. If θ_n denotes the angle between the horizontal and the wavenumber vector of the nth disturbance wave, the resonance condition is

$$\cos\theta_n + \cos\theta_{n+1} = \cos\theta. \tag{3}$$

Expressions for $\cos\theta_n$ and $\cos\theta_{n+1}$ can be obtained from (2) when $M = 0$:

$$\cos\theta_n = |-\alpha\sin\beta\sin\theta + (\alpha\cos\beta + n)\cos\theta|\,[(\alpha\sin\beta)^2 + (\alpha\cos\beta + n)^2]^{-\frac{1}{2}}. \tag{4}$$

Mied showed that (4) yields in fact particular (α, β)-pairs which satisfy the resonance condition (3) and yield $\lambda_r > 0$ for finite-amplitude basic waves.

3. Numerical approach and remarks on the nature of the instabilities

A numerical solution of (2) can be found by truncating the Fourier series in (1) at $n = \pm N$, where N now denotes a sufficiently large integer. Then (2) becomes a finite system of homogeneous equations for (ψ_n, b_n). In a further step, Mied (1976) has eliminated b_n so that the resulting eigenvalue problem includes terms that are quadratic in λ. It has been solved by a sophisticated bisection technique, which, however, requires an *a priori* knowledge of the approximate locations of the eigenvalues in the complex λ-plane.

A simpler approach is to solve (2) for $-N \leqslant n \leqslant N$ without eliminating b_n. Then there are several algorithms yielding all eigenvalues and eigenvectors without any *a priori* knowledge of the approximate values of λ. The following results have been obtained by means of the QR algorithm using the eigensystem routines of Smith *et al.* (1976). They were computed with an accuracy better than 10^{-3}, which could always be obtained by taking sufficiently large values for N. In most cases it was possible to choose $N < 15$, so that the order of the coefficient matrix of (2) was $(4N+2) < 62$. Then the execution time on an UNIVAC 1100/82 computer, on which all computations were performed, was always less than 1 min.

First of all we have re-examined Mied's (1976) statement that, although (3) and (4) have two solutions at $\alpha = 0{\cdot}798$ and $\alpha = 6{\cdot}67$ for $\theta = 30°$, $\beta = 90°$ and $n = 0$, growing parametric disturbances will occur only in the vicinity of $\alpha = 0{\cdot}798$. He identified $\alpha = 6{\cdot}67$ as a spurious root not contiguous to a region of parametric instability in the (α, M) parametric space. This statement clearly is in contradiction to Hasselmann's (1967) criterion that nonlinear resonant triads consisting of one finite and two infinitesimal wave components must be unstable for sum interactions. Our computations in fact yield parametric instabilities in the vicinity of $\alpha = 6{\cdot}67$, as shown in figure 2 for a normalized basic state amplitude $M = 0{\cdot}1$. The value $\alpha = 0{\cdot}798$ corresponds to a resonant triangle with one tip on curve C of the interaction diagram (figure 3), whereas $\alpha = 6{\cdot}67$ corresponds to a triangle with a tip on curve B (Mied 1976). Also, for $\theta = 30°$, $\beta = 90°$ and $n > 0$, there are always two roots satisfying (3) and (4). The related resonant triads extend along curves A and B of the interaction diagram. The α-values for curve A are 0·933 for $n = 1$, 1·65 for $n = 2$ (Mied 1976); along curve B we obtain $\alpha = 19{\cdot}8$ for $n = 1$ and $\alpha = 33{\cdot}0$ for $n = 2$. In agreement with Hasselmann (1967) we again find parametric instabilities that are characterized by maximum growth rates λ_r close to these values (figure 2). It should be mentioned that, for $\theta = 30°$, there are occasionally up to four resonant triads for given values of β and n which give rise to four different parametric instabilities.

The above results can be generalized for arbitrary values of θ and β. For sufficiently large $|n|$ and $0 < \beta < 180°$, (4) yields

$$\cos\theta_n \sim \cos\theta_{n+1}. \tag{5}$$

We then have approximately $\cos\theta_n = \frac{1}{2}\cos\theta$ from (3), so that (4) becomes a quadratic in α whose discriminant d is

$$d = 4n^2 \sin^2\beta \cos^2\theta(3 + \sin^2\theta).$$

For large $|n|$, (3) and (4) thus always have two real roots for β and θ within the open intervals (0, 180°) and $(-90°, 90°)$ respectively. Both roots define two curves in the (α, β)-plane; an example for $\theta = 30°$ and $n = 10$ is shown in figure 4. Note that both curves A and B were not obtained by using the asymptotic relation (5) but represent exact numerical solutions of (3) and (4). The discontinuities in the curves are general features occurring at

$$\beta_{A,B} = \arccos(\pm\tfrac{1}{2}\cos\theta) - \theta, \tag{6}$$

in the limit of large n. Their physical meaning will immediately become clear. Curves A and B define two families of triads each following one of those curve segments in the resonant-interaction diagram which extend to infinity and are correspondingly denoted by A and B in figure 3 (for further interaction diagrams see Phillips 1969).

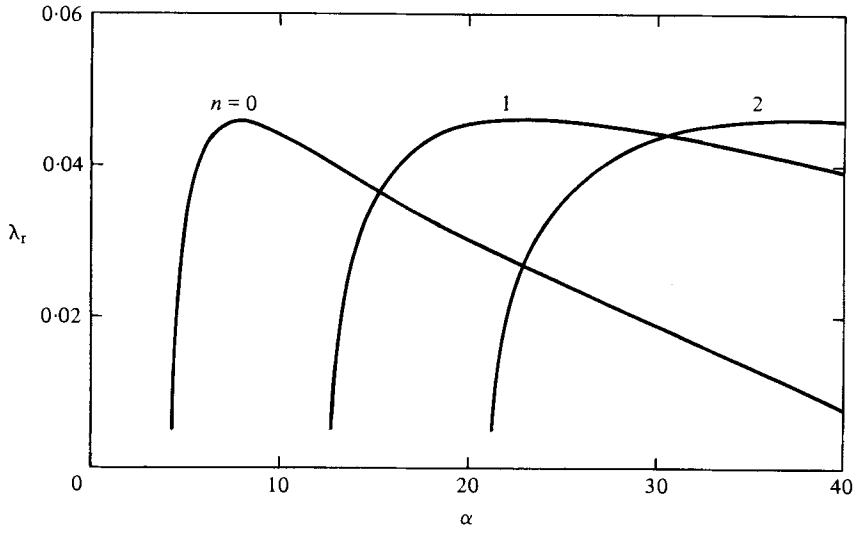

FIGURE 2. Computed growth rates λ_r versus magnitude α of Floquet vector, for $n = 0$, 1 and 2, when $\theta = 30°$, $\beta = 90°$ and $M = 0{\cdot}1$. Note that λ_r, α and M have been non-dimensionalized by the Brunt–Väisälä frequency and the basic-state wavenumber.

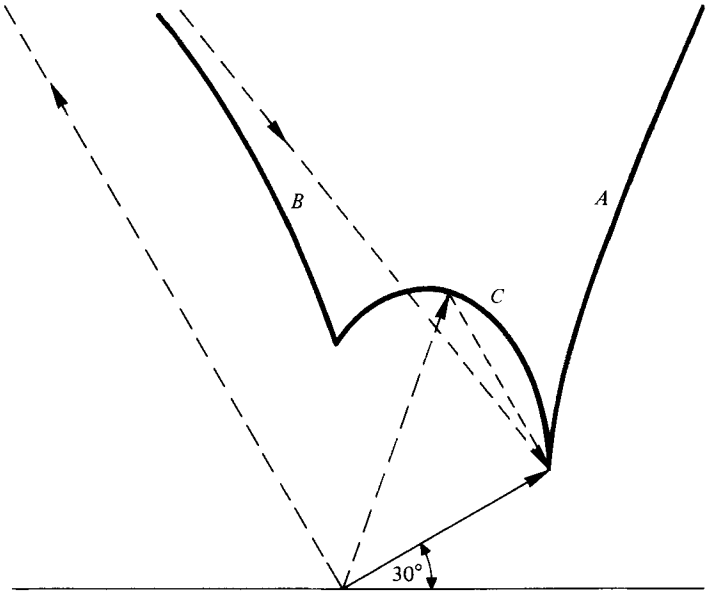

FIGURE 3. Resonant-interaction diagram (after Phillips 1969). The curve segments A, B and C define the nonlinear resonant sum interactions of two disturbance waves with a basic-state wave propagating at an angle of 30° to the horizontal. For a basic-state wave with a vanishingly small amplitude M, an unstable disturbance wave always participates in a nonlinear resonant interaction with the basic wave. The resonant triangle with a tip on curve C gives rise to a parametric instability at $\alpha = 0{\cdot}798$, $\beta = 90°$ and $n = 0$. The second resonant triangle has a tip on curve B and corresponds to a parametric instability at $\alpha = 6{\cdot}67$, $\beta = 90°$ and $n = 0$.

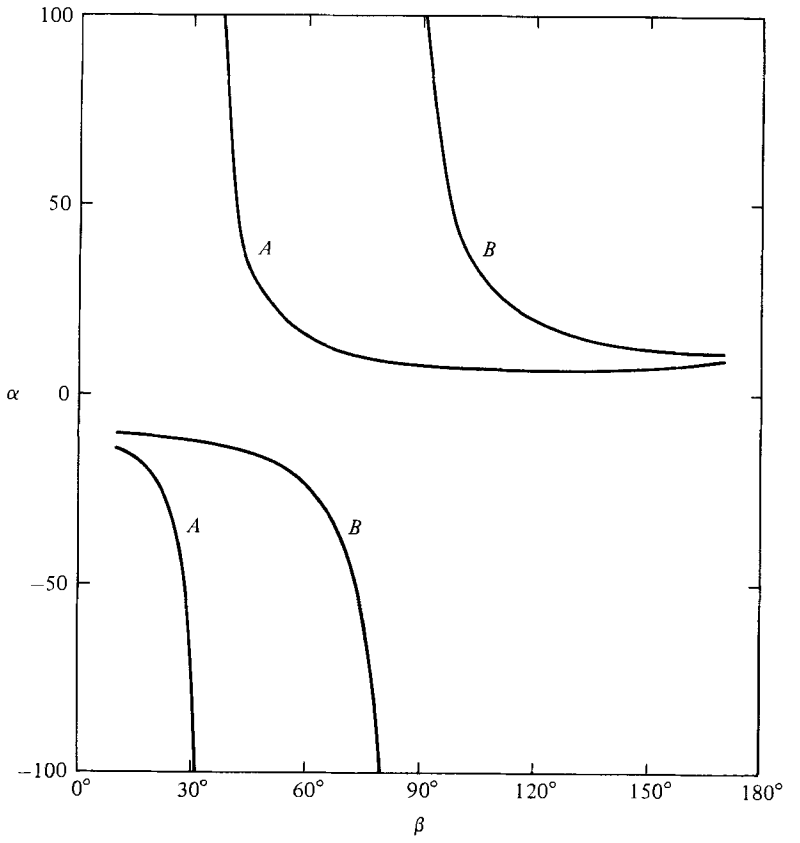

FIGURE 4. Solution curves satisfying (3) and (4) for $\theta = 30°$ and $n = 10$. Points on curve A (B) define resonant triads extending along curve segment A (B) of the interaction diagram shown in figure 3.

The angles formed by both curve segments with the horizontal asymptotically become $\arccos(\pm\frac{1}{2}\cos\theta)$, showing that the discontinuities in the (α,β)-plane occur whenever β approaches the direction of curve segment A or B of the interaction diagram.

It should be mentioned that the results for $-180° < \beta < 0°$ are related to those for $0° < \beta < 180°$ by the transformation

$$(\alpha,\beta)\rightarrow(-\alpha,\beta-180°), \tag{7}$$

which does not alter (2) and (4). Similarly, the results for $n < 0$ can be obtained from those for $n > 0$ by the transformation

$$(n,\alpha)\rightarrow(-n,-\alpha); \tag{8}$$

then (4) remains unaltered, and (2) yields

$$\lambda(-\alpha) = \lambda^*(\alpha), \quad (\psi_{-n}(-\alpha), b_{-n}(-\alpha)) = (\psi_n^*(\alpha), b_n^*(\alpha)),$$

where the asterisk denotes complex conjugates. The results for negative θ can be obtained from those for positive θ or vice versa, since the transformation

$$(\theta,\beta)\rightarrow(-\theta,-\beta) \tag{9}$$

leaves (4) unaltered, and yields

$$\lambda(-\theta, -\beta) = \lambda(\theta, \beta), \quad (\psi_n(-\theta, -\beta), b_n(-\theta, -\beta)) = (-1)^n (\psi_n(\theta, \beta), b_n(\theta, \beta)),$$

from (2).

In the following we shall denote the parametric instabilities by A or B depending on the curve segment along which the related resonant triangles extend in the limits of large $|n|$ and small amplitudes M. For $n = 0$, the tip of a resonant triangle may lie along curve segment C of the interaction diagram. For simplicity we shall associate the corresponding instability with family A or B depending on the curve segment to which the resonant triangles move with increasing $|n|$. According to Phillips (1966), the interaction times for nearly collinear waves are shorter than those for nearly equilateral waves. Therefore we expect that, for $\theta = 30°$, the maximum growth rates of A-instabilities are in general greater than those of B-instabilities.

4. Maximum growth rates

It is reasonable to assume that, if at all, the disturbance waves with the largest growth rates should be the ones most easily observed in atmospheric and oceanic flows. Therefore we shall now concentrate on some properties of maximum growth rates $\Lambda_r = \max(\lambda_r(\alpha))$ which can be interpolated by a quadratic using three computed points in the (α, λ_r)-plane.

Growth rates of A- and B-instabilities as functions of α for $\theta = 30°$, $\beta = 90°$ and $n \leqslant 2$ are shown in figure 7 of Mied (1976) and in figure 2 of this paper respectively. Both figures indicate that, for constant amplitude M of the basic wave, the maximum growth rates tend to increase with higher modenumber n. Figure 5 shows in fact that the maximum growth rates of A- and B-instabilities converge monotonically with increasing n. It should be mentioned that, for the particular parameters chosen in figure 5, the growth rates of the B-instabilities can be computed with an accuracy of 10^{-3} only for $n \leqslant 3$ if the Fourier series in (1) is truncated at $n = \pm 15$. The reason is that the corresponding resonant triads have relatively large α values which, in turn, are due to the fact that $\beta = 90°$ is close to the discontinuity point $\beta_B = 86°$ resulting from (6) for $\theta = 30°$. It will be shown below, however, that the limitation to small modenumbers n in the case of large α does not impose severe restrictions to the use of the truncated Fourier series approximation.

Up to this point, β was fixed to 90°. We now vary β for a given basic state with $\theta = 30°$ and $M = 0{\cdot}1$ to find $\max(\Lambda_r(\beta))$, i.e. those directions β at which the fastest growing disturbance waves occur. The results for $10° \leqslant \beta \leqslant 170°$ and $n = 0$, 1, 4 and 10 are shown in figure 6 and can be summarized as follows.

(*a*) For n = constant, Λ_r has absolute maxima at $\beta = 34°$ for A-instabilities, and at $\beta = 86°$ for B-instabilities. These angles are identical with the asymptotic angles of the infinite curve segments A and B in the resonant-interaction diagram.

(*b*) With increasing n, Λ_r converges to the limits 0·0517 for A-instabilities and 0·0462 for B-instabilities. The computations show within an accuracy of 10^{-3} that both limits do not depend on β. For any given β, the convergence is the faster the closer β is to β_A or β_B, depending on the type of the instability.

(*c*) With β = constant, Λ_r increases monotonically with n for A-instabilities, whereas it may vary non-monotonically at small n in the case of B-instabilities.

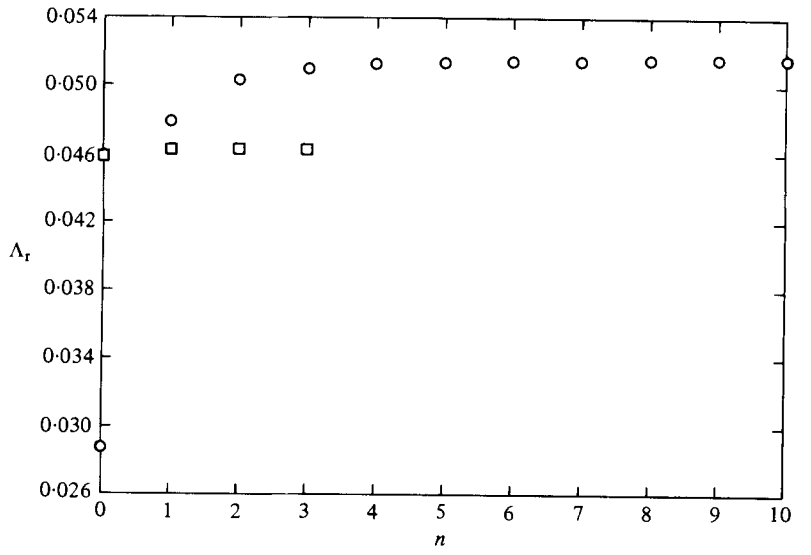

FIGURE 5. Maximum growth rates Λ_r versus modenumber n, for $\theta = 30°$, $\beta = 90°$ and $M = 0{\cdot}1$. Instabilities of type A (circles) asymptote to $\Lambda_r = 0{\cdot}0517$, those of type B (squares) to $\Lambda_r = 0{\cdot}0462$. Growth rates of B-instabilities have only been computed for $n \leqslant 3$ for reasons explained in the text.

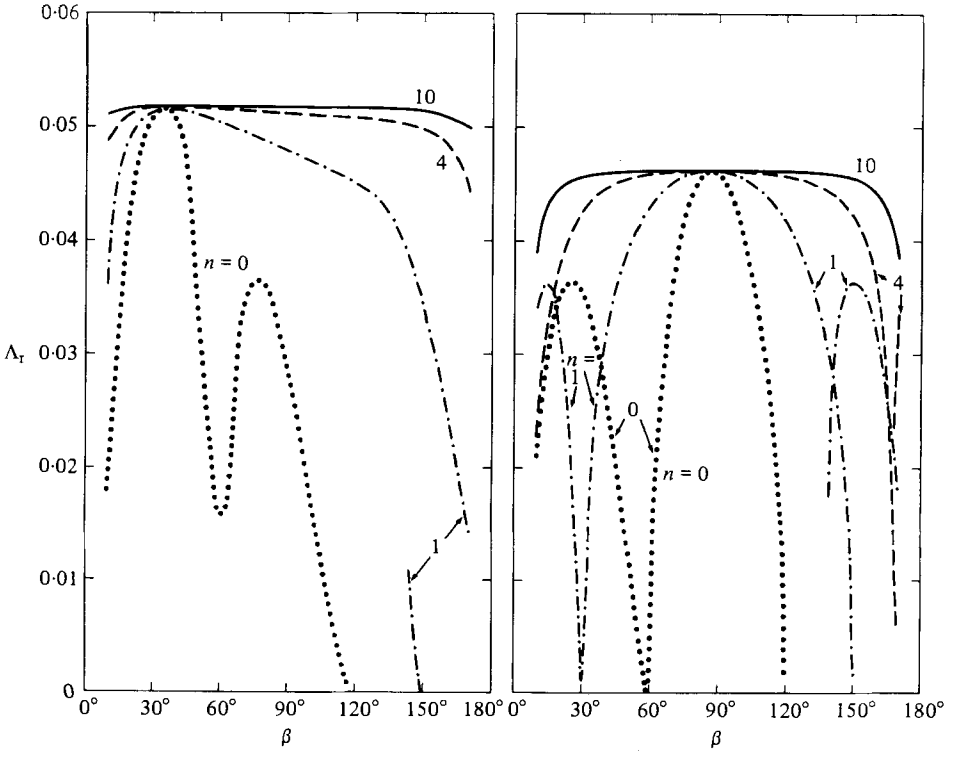

FIGURE 6. Maximum growth rates Λ_r of A-instabilities (left) and B-instabilities (right) versus direction β of the Floquet vector, for several modenumbers n. Here $\theta = 30°$ and $M = 0{\cdot}1$. With increasing n, the growth rates of A- (B-) instabilities asymptotically approach the limit $\Lambda_r = 0{\cdot}0517$ ($0{\cdot}0462$), which does not depend on β. At $n = 1$ and $\beta \simeq 145°$, four unstable disturbances occur simultaneously.

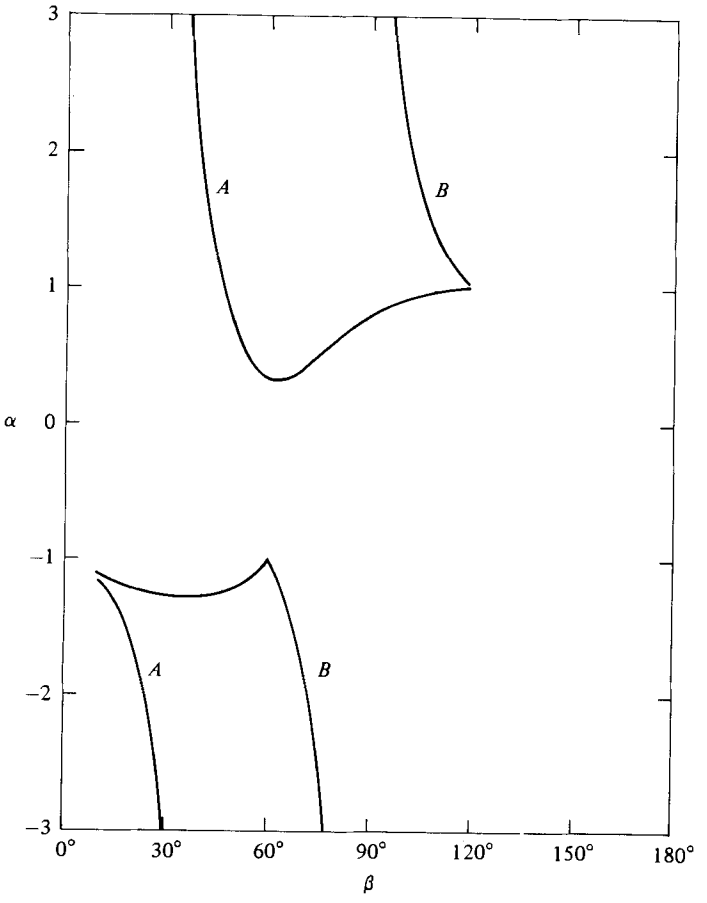

FIGURE 7. Loci of maximum growth rates of A- and B-instabilities in the (α, β)-plane for $n = 0$. Both curves end at $\beta = 120°$ because for $n = 0$ no resonant triads and parametric instabilities exist at larger angles.

(*d*) For $n = 0$, there are no parametric instabilities at $\beta \geqslant 120°$ because $\cos\theta_0 \geqslant \cos\theta$, i.e. no resonant triads can exist. If there are four resonant triads at particular (n, β)-pairs, as mentioned in § 3, four parametric instabilities may also exist simultaneously. In figure 6, this happens at $n = 1$ and $\beta \sim 145°$.

(*e*) Results for $-170° \leqslant \beta \leqslant -10°$ and/or $n < 0$ can be easily obtained by applying the transformations (7) and (8). From (9) we can get results for $\theta = -30°$, which may be useful for applications in the atmosphere where the phase of internal gravity waves in general propagates downward.

The computations have shown that the maximum growth rates Λ_r always occur at α-values close to those obtained from (3) and (4) for the related resonant triads. The maximum growth rates define two curves in the (α, β)-plane which, for large $|n|$, look very much like those in figure 4 except that the values at the ordinate depend on n. There are, in particular, discontinuities at $\beta = 34°$ for A-instabilities and $\beta = 86°$ for B-instabilities, so that the absolute maxima of Λ_r shown in figure 6 coincide with infinitely large values of $|\alpha|$. To explain further details of figure 6 we consider the loci of maximum growth rates in the (α, β)-plane for $n = 0$ (figure 7). Besides the familiar

discontinuities, both curves show minima of $|\alpha|$ near $\beta = 60°$ which cause the minima of the $n = 0$ growth rate curves at the same angle. The secondary maxima of the $n = 0$ growth rate curves at $\beta = 75°$ and $25°$, respectively, are not correlated with any particular features in figure 7. They obviously result from the local minima at $\beta \simeq 60°$ and a general tendency of the growth rate curves to decrease with increasing values of $|\beta - \beta_A|$ and $|\beta - \beta_B|$ respectively. The $n = 1$ maximum-growth-rate curve for B-instabilities shows a maximum at $\beta = 15°$ and a minimum at $\beta = 30°$ which can be explained in the same way, whereas the maximum at $\beta = 150°$ is due to the fact that four parametric instabilities exist simultaneously.

The convergence speed of the Fourier series in (1) turned out to decrease with increasing $|\alpha|$. Thus the convergence is particularly slow for β-values near the discontinuity points β_A and β_B, so that the available computer core and time prohibit the solution of (2) for large modenumbers $|n|$. Figures 5 and 6 indicate, however, that, for $\beta \sim \beta_A$ or $\beta \sim \beta_B$, Λ_r converges rapidly to the corresponding limits with increasing $|n|$, rendering computations with large $|n|$ unnecessary.

5. Concluding remarks

Our investigations have added to Mied's (1976) results in three ways.

(*a*) The numerical approach has been improved, so that for a basic internal gravity wave of given amplitude and propagation direction the properties of parametric instabilities can be studied for all magnitudes and directions of the Floquet vector at reasonable expense. It should be mentioned, however, that the eigensystem methods would work even more efficiently if they were fitted to the particular band structure of the coefficient matrix in (2).

(*b*) The improved numerical approach allowed us to discard the concept of spurious roots and to find those parametric instabilities that have their origin in the resonant triads lying along branch B of the interaction diagram. It is not yet clear why Mied has missed these solutions. Substitution of the corresponding roots into his equation (14) may reveal whether these solutions got lost by eliminating b_n from the interaction equations or whether his search strategy simply did not cover the relevant parameter space.

(*c*) By removing the restriction $\beta = 90°$ and extending the number of Fourier components we have confirmed the suggestion that the disturbance waves with the largest wavenumbers are the most unstable ones. These disturbances always propagate in two particular directions, which coincide with the directions of the two infinite curve segments in the resonant interaction diagram. With increasing wavenumber, the maximum growth rates converge to limits that depend on the propagation direction. The disturbance waves propagating at the smaller angle to the basic wave grow at the larger rate.

These results were obtained for inviscid fluids. In viscous fluids, the effect of dissipation is proportional to the square of the disturbance wavenumber, i.e.

$$k_n^2 = (\alpha \sin\beta)^2 + (\alpha \cos\beta + n)^2.$$

Thus, for any given value of β, the maximum growth rate Λ_r no longer converges with increasing n, as shown in figure 5, but decreases rapidly for mode-numbers n comparable to or larger than some critical value n'. This critical value is deter-

mined by a disturbance wavenumber $k_{n'}$, which produces viscous decay rates of the order of the growth rates obtained when dissipative effects are neglected. The value of n' depends on β, so that the curves shown in figure 6 are affected considerably by dissipative effects. In the neighbourhood of the discontinuity points β_A and β_B, for instance, the curves must undergo drastic changes because k_n becomes extremely large.

The author thanks Professor K. C. Yeh of the University of Illinois for helpful discussions.

REFERENCES

ABRAMOWITZ, M. & STEGUN, I. A. 1965 *Handbook of Mathematical Functions*. Dover.

DRAZIN, P. G. 1977 On the instability of an internal gravity wave. *Proc. R. Soc. Lond.* A **356**, 411–432.

GILL, A. E. 1974 The stability of planetary waves on an infinite beta-plane. *Geophys. Fluid Dyn.* **6**, 29–47.

HASSELMANN, K. 1967 A criterion for nonlinear wave stability. *J. Fluid Mech.* **30**, 737–739.

KLOSTERMEYER, J. 1978 Nonlinear investigation of the spatial resonance effect in the night-time equatorial F region. *J. Geophys. Res.* **83**, 3753–3760.

LORENZ, E. N. 1972 Barotropic instability of Rossby wave motion. *J. Atmos. Sci.* **29**, 258–264.

MCEWAN, A. D. & ROBINSON, R. M. 1975 Parametric instability of internal gravity waves. *J. Fluid Mech.* **67**, 667–687.

MIED, R. P. 1976 The occurrence of parametric instabilities in finite-amplitude internal gravity waves. *J. Fluid Mech.* **78**, 763–784.

MIED, R. P. 1978 The instabilities of finite-amplitude barotropic Rossby waves. *J. Fluid Mech.* **86**, 225–246.

PHILLIPS, O. M. 1966 Internal wave interactions. In *Proc. 6th Symp. Nav. Hyd.* (ed. R. D. Cooper & S. W. Doroff), pp. 535–544. Office of Naval Research, Dept. Navy, Publ. ARC-136.

PHILLIPS, O. M. 1969 *The Dynamics of the Upper Ocean*. Cambridge University Press.

SMITH, B. T., BOYLE, J. M., DONGARRA, J. J., GARBOW, B. S., IKEBE, Y., KLEMA, V. C. & MOLER, C. B. 1976 *Matrix Eigensystem Routines–EISPACK Guide*. Springer.